Microstructural Evolution during the Dynamic Deformation of High Strength Navy Steels

Final Report

Submitted by:

K.S. Kumar
Division of Engineering
Brown University
Providence, RI 02912

Submitted to:

Materials Division
Office of Naval Research
Arlington, VA 22217

REPORT DOCUMENTATION PAGE

Form Approved
OMB No. 0704-0188

PLEASE DO NOT RETURN YOUR FORM TO THE ABOVE ADDRESS.

1. REPORT DATE *(DD-MM-YYYY)*	2. REPORT TYPE	3. DATES COVERED *(From - To)*
19-05-2008	Final Technical	15-11-04 to 31-12-07

4. TITLE AND SUBTITLE

Microstructural Evolution During Dynamic Deformation of Low C-10Ni-Cr-Mo-V Steels

5a. CONTRACT NUMBER

NA

5b. GRANT NUMBER

N00014-05-1-0062

5c. PROGRAM ELEMENT NUMBER

NA

6. AUTHOR(S)

Sharvan Kumar

5d. PROJECT NUMBER

NA

5e. TASK NUMBER

NA

5f. WORK UNIT NUMBER

NA

7. PERFORMING ORGANIZATION NAME(S) AND ADDRESS(ES)

Brown University
Division of Engineering
Box D
Providence, RI 02912

8. PERFORMING ORGANIZATION REPORT NUMBER

Final

9. SPONSORING/MONITORING AGENCY NAME(S) AND ADDRESS(ES)

Office of Naval Research Regional Office Boston
495 Sumner Street Room 627
Boston, MA 02210-2109

10. SPONSOR/MONITOR'S ACRONYM(S)

NA

11. SPONSOR/MONITOR'S REPORT NUMBER(S)

NA

12. DISTRIBUTION/AVAILABILITY STATEMENT

Approved for Public Release; Distribution is Unlimited

13. SUPPLEMENTARY NOTES

None

14. ABSTRACT

We have characterized the propensity for adiabatic shear band formation (an associated microstructural evolution) under dynamic deformation conditions in an ultra-high strength (160 Ksi/1.1GPa) Fe-10 Ni-0.1C-Cr,Mo,V steel and demonstrated that this steel is highly prone to shear localization and failure. In the as-received condition, the steel has a lath martensite microstructure. During dynamic deformation, shear localization occurs and manifests by an optically visible shear band; the original microstructure is discernible within the band. With progression in severity of localization, there is evidence for a central region within the shear band composed of ~300 nm size equiaxed grains constituting austenite, with a low dislocation content, and heavily twinned ferrite. In the extreme situation, a crack "chases" the shear band, and examination of the resulting fracture surfaces provides evidence for the presence of a thin liquid film layer. We have also observed that lowering the Ni content in the alloy significantly and adding Cu to the alloy, enables improvements in resistance to shear localization, both in terms of initiation and propagation of the shear band.

15. SUBJECT TERMS

adiabatic shear band formation, dynamic deformation, ultra-high strength 10Ni steel, microstructural evolution, lath martensite microstructure, shear localization

16. SECURITY CLASSIFICATION OF:			17. LIMITATION OF ABSTRACT	18. NUMBER OF PAGES	19a. NAME OF RESPONSIBLE PERSON
a. REPORT	b. ABSTRACT	c. THIS PAGE			Sharvan Kumar
U	U	U	UU	35	19b. TELEPHONE NUMBER *(Include area code)* 401-863-2862

Executive Summary

We have characterized the propensity for adiabatic shear band formation under dynamic deformation conditions in an ultra-high strength (160 Ksi/1.1GPa) 10Ni steel and demonstrated that in spite of its outstanding static toughness, this steel is highly prone to shear localization and failure.

Specifically, microstructural evolution during deformation of a Fe-10 Ni-0.1C-Cr,Mo,V steel was examined. In the as-received condition, the steel has a lath martensite microstructure, and during quasi-static deformation, shear appears to be accommodated by lath rotation and lath thinning. During dynamic deformation, shear localization occurs and manifests by an optically visible shear band. Initially, the original microstructure is discernible within the band. With progression in severity of localization, there is evidence for a central region within the shear band composed of ~300 nm size equiaxed grains constituting austenite, with a low dislocation content, and heavily twinned ferrite. In the extreme situation, a crack "chases" the shear band, and examination of the resulting fracture surfaces provides evidence for the presence of a thin liquid film layer. Together, these observations provide a microstructural footprint for deformation progresses evolution shear localization, and a sense for the accompanying thermal profile within the shear band.

In the later part of this current three-year effort, we have also observed that lowering the Ni content in the alloy significantly (down to about 2-3%Ni: HSLA-Comp2 and 3) and adding Cu to the alloy, enables improvements in resistance to shear localization, both in terms of initiation and propagation of the shear band.

It is our expectation that this study will complement and provide vital microstructural information and understanding to the on-going efforts on this problem at other institutions where the experimental mechanics (CalTech), theoretical models (NC State) and first principles alloy design (Northwestern) are the focus.

Title page

Executive Summary 2

Table of Contents 3

1.0 Background 4

2.0 Program Results and Analysis 7

2.1 Deformation of the 10Ni-0.1C Steel 7

2.2 Deformed Microstructure following Quasi-static Compression 8

2.3 Deformed Microstructure following Dynamic Compression Deformation 11

2.4 Deformation Response of HSLA-Comp 3 and HSLA-Comp 2 25

3.0 Conclusions 32

4.0 References 34

1.0 Background

Improved ship protection at reduced weight for design against future weapon threats will demand alloy steels in the 130-150 Ksi range. In considering the threats posed to the ship protection system, a possible classification on the basis of strain rates would be: a) underwater shock (corresponding to strain rates of around 10^2 s^{-1}), b) air blast (corresponding to strain rates of around 10^3 s^{-1}), and c) fragment penetration (corresponding to strain rates of around 10^5 s^{-1}). Metallurgical evaluation of the dynamic response (in these strain rate regimes) of such steels and their variants formed the basis of the three-year effort completed in December 2007 and the scientific outcomes are summarized in this final report. The relevant theory and a detailed characterization of the dynamic response of these steels continue to be developed at the California Institute of Technology (CalTech) in a parallel effort. A significant outcome of the effort at Brown University is the provision of a strong physical metallurgy basis to the detailed mechanics understanding being obtained through the CalTech program, thereby enabling alloy design for specific naval applications that require enhanced blast resistance and fragmentation armor capabilities.

When materials are deformed at high strain rates, as in many ballistic applications, a phenomenon that manifests itself frequently is the formation of narrow zones of highly localized deformation known as adiabiatic shear bands (ASB). Whether or not it is accompanied by fracture, such localization usually implies failure of the structural component through a loss in the load-carrying capacity of the highly deformed material within the shear band [1]. Shear bands have been observed in machining, ballistic impact, high-velocity forming etc and in a variety of materials including alloys of Cu, Al, Ti and steels. Such shear bands arising from localization of deformation occur more readily in materials with a low work-hardening rate, low strain-rate sensitivity, low thermal conductivity and a high thermal softening rate. Traditionally, shear bands have been classified into two types, deformed bands and transformed bands, the latter suggestive of a transformation having occurred within the band during (or after) its formation [2,3]. According to this classification, transformed bands in steels may be as narrow as 5-10 μm and will appear white after etching with a Nital solution. The transformation is thought to be austenite to martensite, due to quenching by the surrounding colder steel although all evidence to date is indirect. In contrast, deformed bands in steels are generally broad and do not etch white. Temperature rise within the

shear bands have been measured using infrared detectors and have been reported to be as high as 600°C [1,4]. More recently, Guduru et al [5] used a newly-developed infrared high speed camera to demonstrate the presence of highly non-uniform temperature distribution along the length of the shear bands with "hot-spots" being present and have questioned the validity of theoretical models that had assume laminar flow [6,7].

Recrystallization arising from high-strain rate loading has been a topic of research interest for several years since the earliest observation of recrystallization in the shear bands in an explosively-loaded steel [8], and its presence has been reported in various materials in association with adiabatic shear bands (ASBs). Reviews on the subject by Murr [9,10], and other research articles [11-19] extensively discuss the origin and underlying mechanisms. Transmission Electron Microscopy (TEM) has been commonly employed to characterize the microstructures of the shear bands for many years, although the narrow dimensions of the shear band width makes the TEM investigation difficult, because specimen perforation generated by ordinary chemical thinning and ion-milling often does not coincide with the band area. In this context, the advent of the FIB (Focussed Ion Beam milling) has enabled the possibility of obtaining specimens from precise locations in the sample. Alternately, the electron backscatter diffraction (EBSD) technique in conjunction with a field emission SEM has also been used to study the microstructural evolution in the shear bands. The technique allows a direct quantitative analysis of the subgrains and substructures as small as 0.2μm, and permits measurements of subgrain/substructure size, misorientation and the distribution of boundary orientation. Xue and Perez-Prado used EBSD to examine microstructural evolution in the shear bands generated using high-strain rates in 304 stainless steel [18] and Ta, and Ta-W alloys[19]. Xue et al found large intragranular misorientation gradients in the shear bands, and employed Taylor factor and misorientation analyses to explain the deformation mechanism [18]. Perez-Prado et al have proposed that the microstructural refinement is not due to boundary mobility-based recrystallization processes, but instead could be attributed to lattice rotations associated with shear localization [19]. Kad and Gebert et al have shown that plastic deformation by shear leads to a strong [11-20] fiber texture prior to the breakup of the existing grain structure [20]. Martinez et al [16] and Lins et al [17] have characterized recrystallization by EBSD in the shear band of Ti-6Al-4V and interstitial free steel respectively. These studies (and more) have attempted to isolate the mechanisms of recrystallization and debated static versus dynamic effects and thermal versus mechanical recrystallization.

The experimental effort summarized in this report has focused primarily on the 10Ni-0.1C-CrMoV steel (both Japanese stock and the US-based heats), although over the last six months of the three-year program, more effort has been devoted to the lower strength HSLA-Comp 2 and Comp 3 alloys being examined at the NSWC-Carderock facility. The effort was coordianated with Dr. Jie Zhang at Carderock, Prof. Ravichandran at CalTech, and Prof. Zikry at North Carolina State with Dr. Julie Christodoulou as the Program Manager. Annual program reviews in the late Spring-early Summer timeframe and focused annual workshops in the late Fall-early-winter timeframe significantly enhanced collaborative efforts and technical updates. Towards the end of the program, additional collaboration was developed with scientists at Los Alamos National Laboratory (Drs. George T. Gray III and Ellen Cerreta) where significant experience, expertise and facilities reside in the area of high-strain rate deformation. Specifically, specimens from the 10Ni-0.1C-CrMoV steel were machined using their "top-hat" configuration and tested and verified the experimental observations made at Brown University.

2.0 Program Results and Analysis

In this Chapter, we summarize the progress we have made in the past three years in understanding the microstructural evolution during dynamic deformation of the 10Ni steel as well as two more-recent steels, HSLA-Comp2 and HSLA-Comp-3.

2.1 Deformation of the 10Ni-0.1C Steel:

The bulk of the characterization work was focused on the as-received material although the quenched material was also characterized for comparison purposes. In the as-received condition, a lath martensitic microstructure was observed (Figure 1a,b); the martensite lath size distribution was measured from several TEM images and the mean lath size is of the order of 55-60 nm (Figure 2). Extraction replicas of carbides were obtained and the composition and the crystal structure of these carbides were determined. The typical carbide size in the extracted replica was < 50 nm and more frequently around 20 nm (Figure 1c). The carbides in the as-received condition were predominantly of the cubic MC-type (M_2C carbides were also observed and were determined to be Mo-rich) although their compositions varied from being predominantly V-rich with small amounts of Ti and Nb dissolved in them through being rich in vanadium and titanium in fairly similar amounts, to being essentially titanium-rich (Figure 3 and Figure 4).

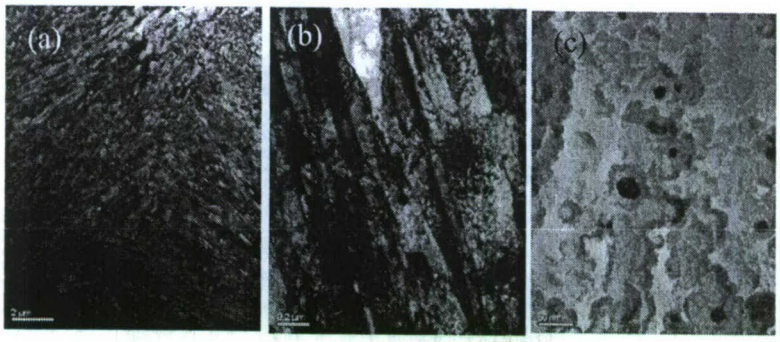

Figure 1a-c: The martensitic lath microstructure (a,b) and the carbide particles as seen in extraction replicas (c).

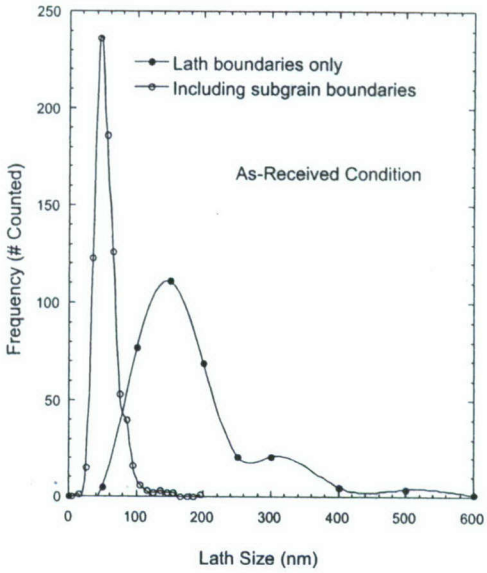

Figure 2: Lath size distribution in the as-received condition in the 10Ni alloy with and without counting the sub-grain boundaries.

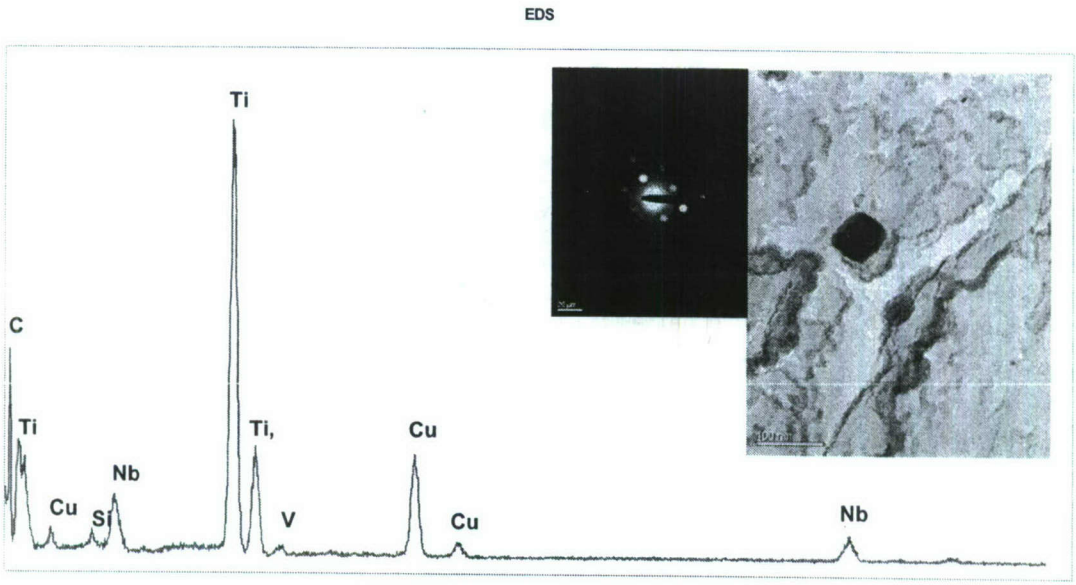

Figure 3: Extraction replica of carbides confirming MC carbide rich in Ti.

2.2 *Deformed Microstructure following Quasi-static Compression*

A series of compression tests using were conducted at room temperature to different compression height strains (15%, 30% and 50%) over a range of quasi-static strain rates (10^{-4} s^{-1}, 10^{-2} s^{-1} and $1s^{-1}$). These large strains lead to specimens losing their axiality and thereby developing intense shearing along the diagonals. This provided an

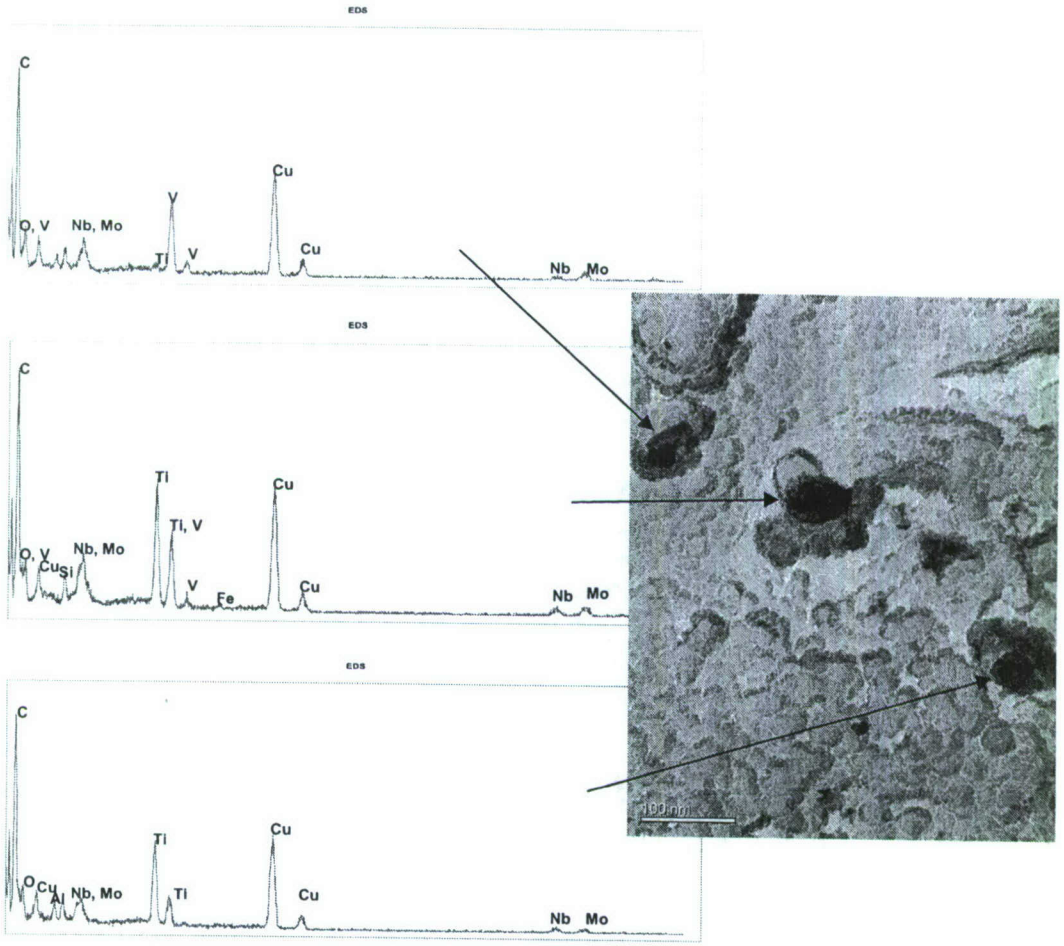

Figure 4: Extraction replica of three MC carbide particles confirming partitioning of Ti and V between them in various ratios.

opportunity to examine the microstructure in these intensely sheared regions. In this highly sheared region, the packets of laths appeared to reorient in the direction of shear (Figure 5a) where as away from the sheared zone the laths appeared to still be in randomly oriented packets. TEM examination of the laths after deformation confirmed this alignment of laths and a refinement in lath size. Representative TEM images of these laths are shown in Figures 5b and 5c following height strains of 30% and 50% respectively at a nominal strain rate of 10^{-2} s^{-1}. The lath size distribution was determined in these intensely sheared zones as a function of strain at a given strain rate (Figure 6a) and as a function of strain rate at a fixed strain (Figure 6b). Also included in Figure 6a, is the lath size distribution for the as-received material and it is evident that following

deformation, there is a refinement in the mean lath size with most of the coarser laths being deformed more readily as would be expected in this size regime. At a fixed level of strain however, strain rate within the quasi-static regime does not appear to have an effect on lath size distribution and in fact, for the three different rates examined, the lath size distribution appears identical (Figure 6b).

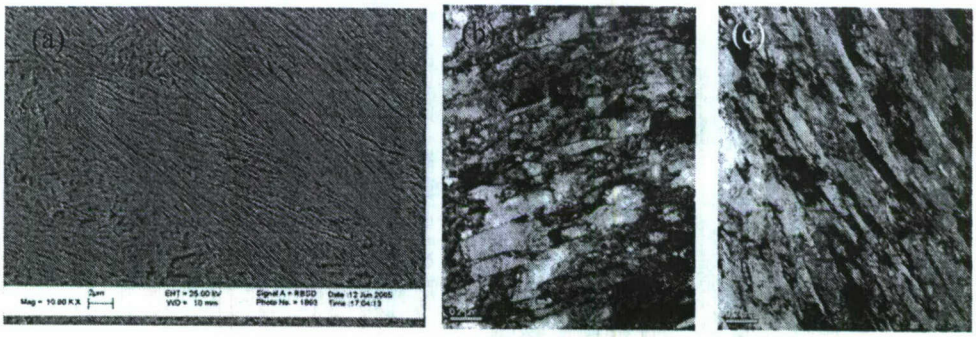

Figure 5: (a) SEM image of the laths in the sheared region for a specimen deformed to 30% height strain at a nominal strain rate of 10^{-2} s^{-1}; (b) TEM image of the laths in the sheared region from specimen in (a), and (c) image of laths in a specimen deformed to 50% height strain at a nominal strain rate of 10^{-2} s^{-1}.

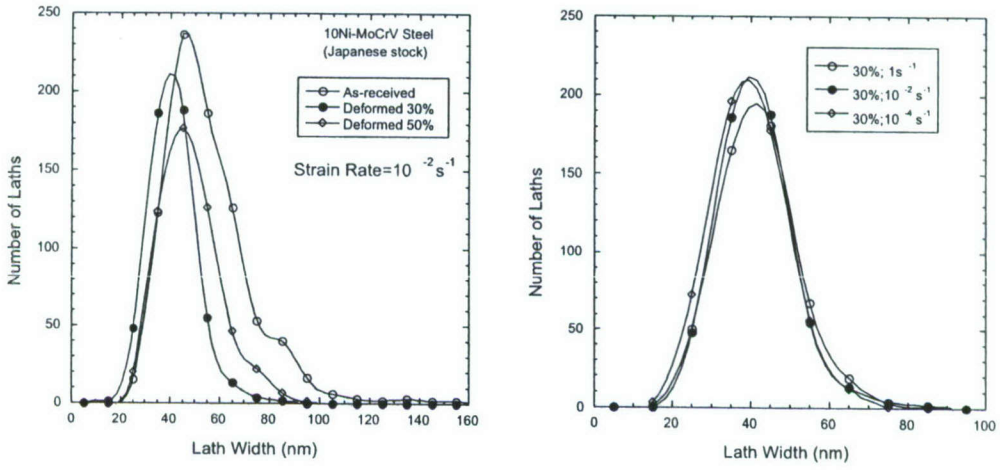

Figure 6: (a) A comparison of the lath size distribution in the as-received condition with those after deformation to a height strain of 30% and 50% at the strain rate of 10^{-2} s^{-1}. In (b) the effect of strain rate (or the lact thereof) on lath size distribution is shown for 30% height strain in all cases.

2.3 *Deformed Microstructure following Dynamic Compression Deformation*

Next, we focused our effort on understanding the dynamic response of this family of alloy. We have subjected compression specimens to a range of strain rates around 10^3 s^{-1} using the Kolsky bar (Hopkinson bar) capability at Brown and have used a combination of projectile length and gas gun pressure to vary strain rates and enable a range of responses. The results are summarized in Figure 7, where combinations of global strain (height reduction) and nominal strain rates examined are illustrated. The first important observation is that there can be considerable localization of deformation and the propensity to form intense shear bands. Examination of the microstructure in the shear band confirms recystallization and hence the fact that these are likely adiabatic shear bands (ASB). Furthermore, we have observed cracking within these ASBs, the extent of severity being dependent on the test condition and varying from small microcracks within the band to splitting of the sample into two pieces. The latter has enabled an examination of the resulting fracture surfaces and these results and observations are highlighted below. The lines in Figure 7 denotes the boundaries between those specimens that exhibited ASBs and cracking versus those that showed localization and shear banding but within which the original microstructure was still evident (transition zone). It is worth noting that this line is a sharp demarcation of the two regions so that at a given strain rate, the transition is quite abrupt.

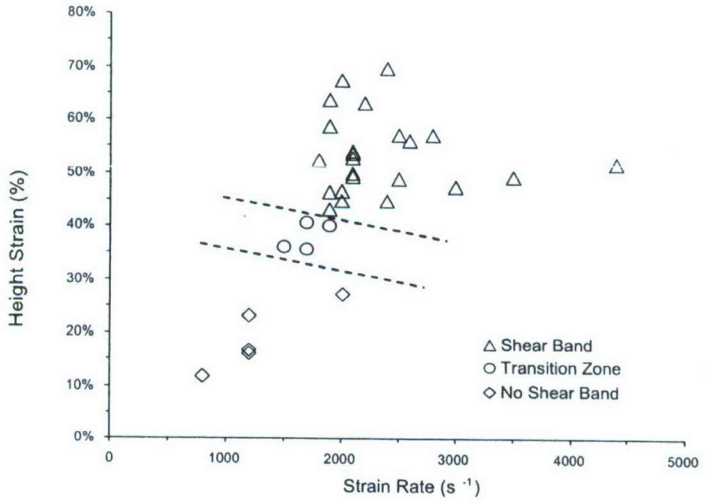

Figure 7: Kolsky/Hopkinson bar compression tests results over a range of strains and strain rates.

Representative quasistatic and dynamic stress-strain curves for the 10 Ni steel are compared in Figure 8 and the characteristic bcc behavior of strain-rate independent work-hardening is seen. It is noted that only the early portion of the dynamic response is shown in this comparison. The complete dynamic test stress-strain curves are shown in Figure 8b for the steel for three different tests and include the localization event as seen by the precipitous drop in stress at height strains corresponding to about 25 percent. Note that stresses as high as 2.0-2.2 GPa are supported prior to localization. However, it should also be remembered that these are engineering stresses and that at a height strain of 25%, significant geometric effects are present and thus the true stress would be lower (this is discussed later in comparison with the HSLA-C3 alloy response).

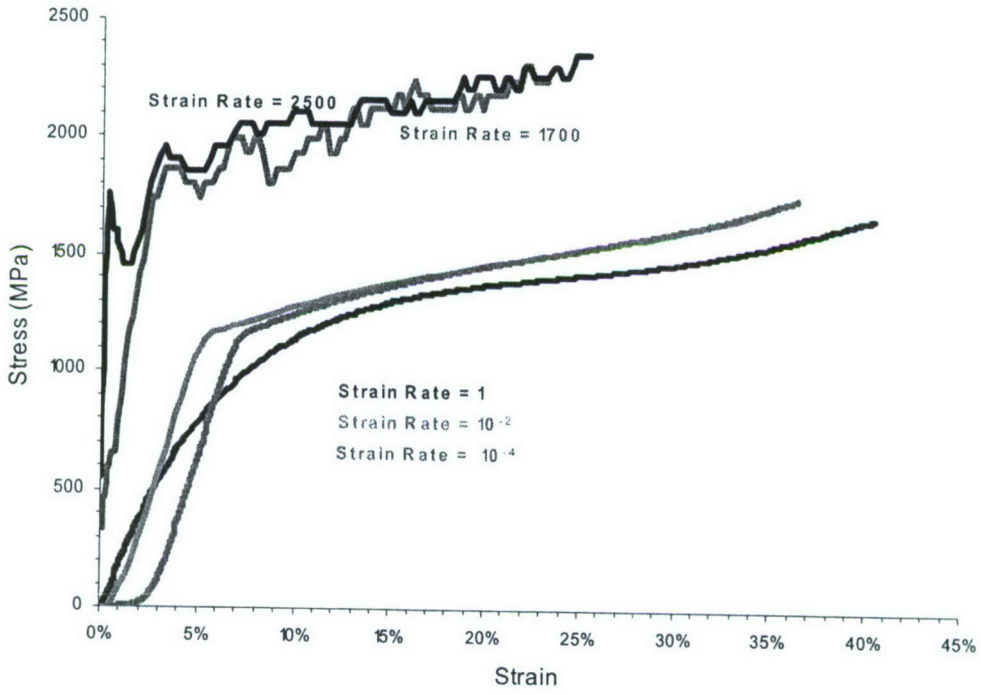

Figure 8: A comparison of the engineering stress-strain curves in compression in the quasi-static versus the dynamic regimes for the 10 Ni steel prior to localization in dynamic deformation.

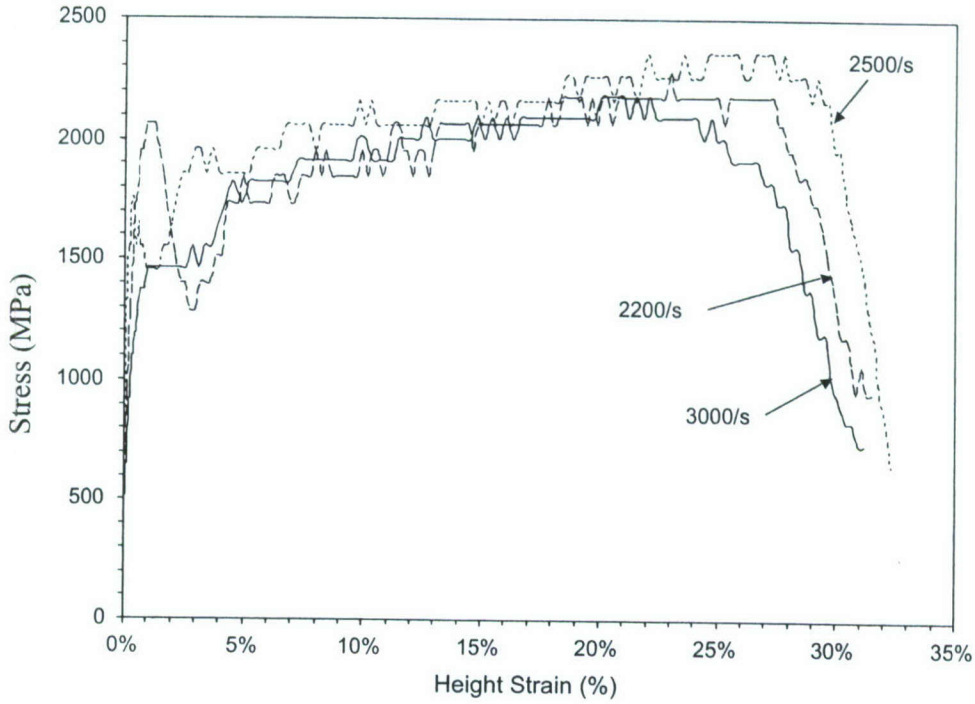

Figure 9: Engineering stress-strain curves in compression in the dynamic regimes for the 10 Ni showing localization in three different instances occurring at height strain of about 25%-30 % consistently.

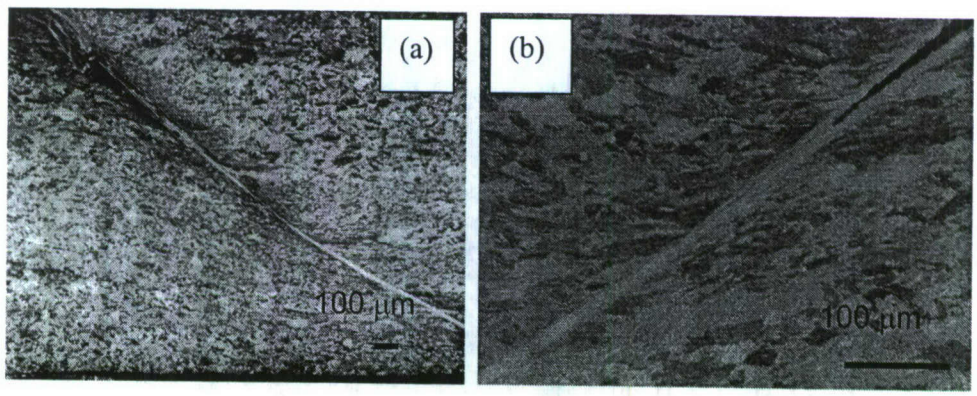

Figure 10: (a) An adiabatic shear band (ASB) in a dynamically deformed 10 Ni specimen (strain rate: 2000/s and height strain of 67%) and (b) a crack within the shear band.

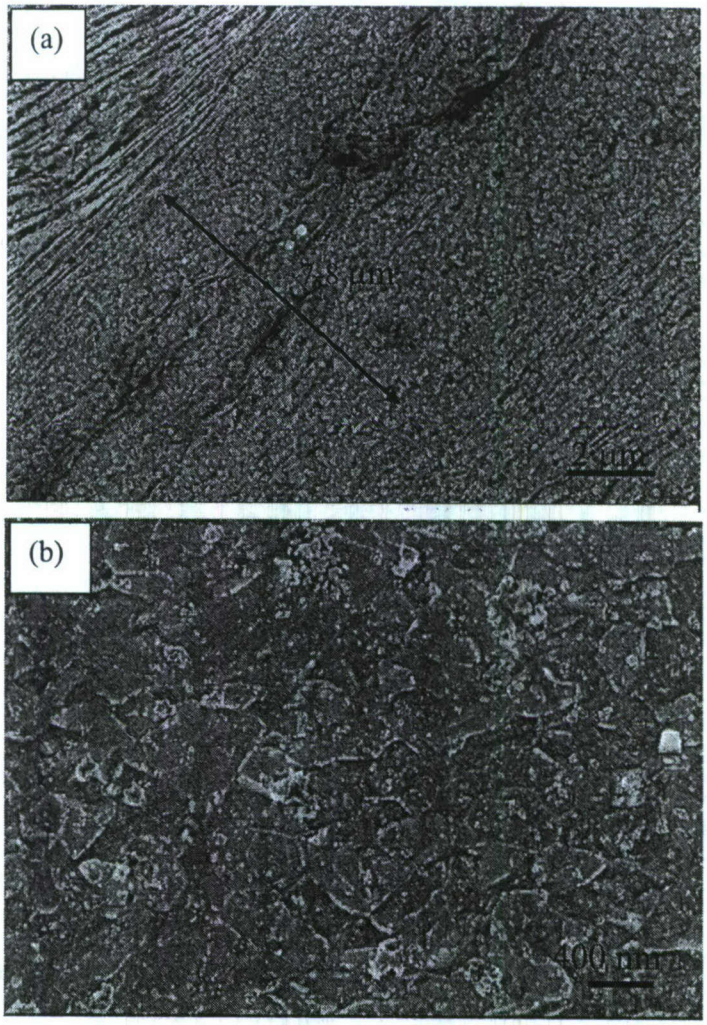

Figure 11 (a) An SEM image of a polished and etched cross-section of a dynamically tested specimen confirming the presence of fine equiaxed grains to the xtent of 7-8 Mm in the center of the adiabatic shear band, and (b) a higher magnification image confirming the equiaxed grains to be of the order of 300-500 nm in size.

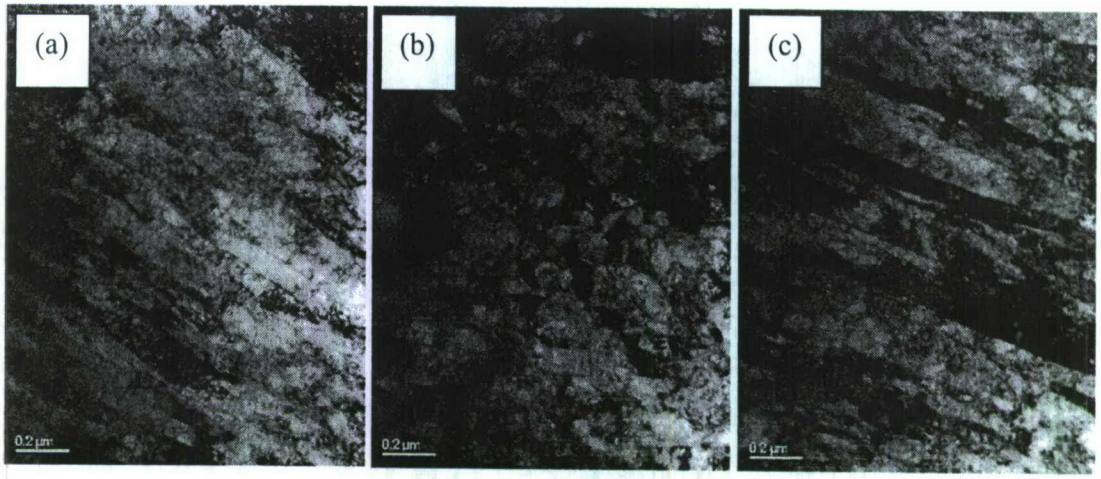

Figure 12: Microstructure across the shear band in a 10 Ni steel (a,c) deformed lath structure and (b) central equiaxed structure.

Microstructurally, the first important observation is that there is considerable localization of deformation and the propensity to form intense shear bands (Figure 10a) that are believed to be adiabatic shear bands (ASBs). Furthermore, we have observed cracking within these ASBs (Figure 10b), the extent of severity being dependent on the test condition and varying from small microcracks within the band to splitting of the sample into two pieces. The fine-scale microstructure across an ASB in a dynamically deformed (2200/s; 63% height strain) 10 Ni steel compression specimen was examined at higher magnifications using an SEM. A central region consisting of fine, equiaxed submicron grains is observed (Figure 11a,b) A cross-section of the deformed specimen was obtained and a thin foil specimen including the adiabatic shear band was also examined in the TEM (Figures 12a-c); the central equiaxed region (Figure 12b) is flanked by a region of highly deformed and oriented lath-like structure (Figures 12a,c). The size distribution of these deformed lath structure is compared to that obtained during quasi-static deformation in Figure 13, and interestingly, the distributions are similar; this is suggestive of a limiting refinement in size below which interfacial energy effects may dominate in destabilizing the structure and leading to the equiaxed structure. It is worth noting that the distribution shown for the as-received material appears similar to the deformed material due to the inclusion of the sub-grain boundaries in the analysis. If the subgrain boundaries are not included in determining the lath size, then the mean size in the as-received condition is almost three times as high at approximately 150 nm.

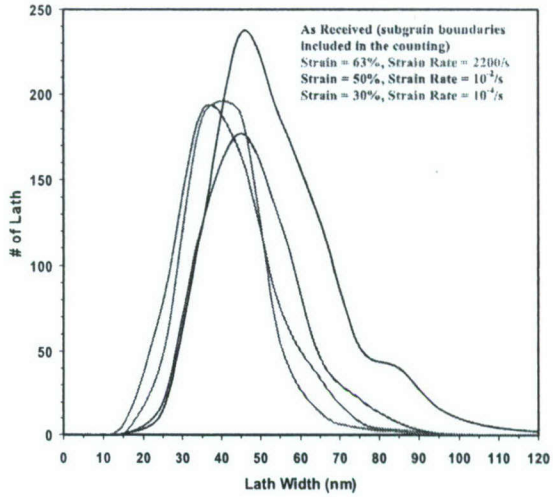

Figure 13: A comparison of the lath size distribution in the as-received, quasi-statically deformed and dynamically deformed conditions.

In order to characterize the structure of the equiaxed grains observed in the central portion of the shear bands, in collaboration with Dr. Mike Miller at Oak Ridge National Laboratory, we used a dual ion beam FIB (Focused Ion Beam) to extract a thin foil specimen for TEM analysis from the shear band. The process is illustrated in Figure 14.

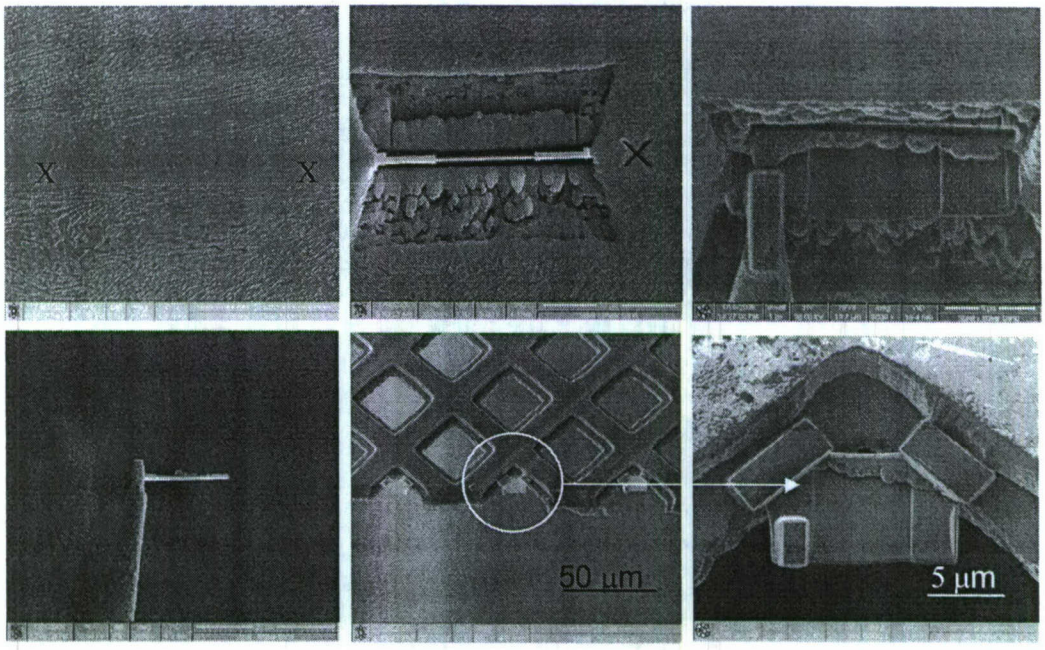

Figure 14: Sequence of steps used to extract a TEM specimen from within the ASB.

Briefly, In Figure 14a, the shear band on a polished specimen surface is demarcated by the two "X" marks. Focussed ion beams are used to precisely trench out material from both sides to leave a thin vertical strip of material which is then milled on both surfaces to produce a "sheet" that is of thickness to be electron transparent (Figure 14b). Next a nanomanipulator arm is attached to the thick side-section using a platinum tab that is bonded to one corner (Figure 14c). The ion beam is then used to detach the specimen from the rest of the sample and it is then transported over to a copper grid (Figure 14d) within the FIB. The 3-mm copper grid was previously cut in half carefully such that the cut leaves a row of "V" shaped cu wires (i.e. we cut the grid along the diagonal of the small squares) as seen in Figure 14e. The specimen is nestled at the root of the "V" and then platinum tabs are applied to bond the specimen to the grid (Figure 14f). The specimen, if thin enough, is ready for observation in the TEM. In our case, the specimen was not electron-transparent and therefore was placed in a precision ion polishing system and further thinned for about 2-3 minutes duration and then examined in the microscope.

Microstructural observations are summarized in Figures 15 and 16. As seen in the images in Figure 15, equiaxed grains roughly 200 nm in size are observed consisting of a low dislocation density and coarse twins. Microdiffraction confirms an fcc structure (austenite) and twinning of the type {111}<11-2>. Two-beam condition images from the matrix and the twin reveal reverse contrast images as expected. Thus, the presence of equiaxed austenite grains in the shear band suggests that the martensite transformed to austenite during the shearing process. It is interesting to note that the austenite did not revert back to martensite upon cooling although this material has a high hardenability and the heat extraction rate from the shear band is thought to be quite rapid. This is likely to be a consequence of the fine austenite grain size which suppresses martensite formation, and previous work on binary Fe-Ni alloys using rapid solidification processing has in fact confirmed this to be the case for grain sizes less that about one micrometer [21-24]. Chemical analysis using EDX spectra from individual grains has confirmed the transformation from martensite to austenite, to a first approximation, to be partitionless so that the average composition of the austenite phase was around 11.5%Ni which is close to the overall alloy composition.

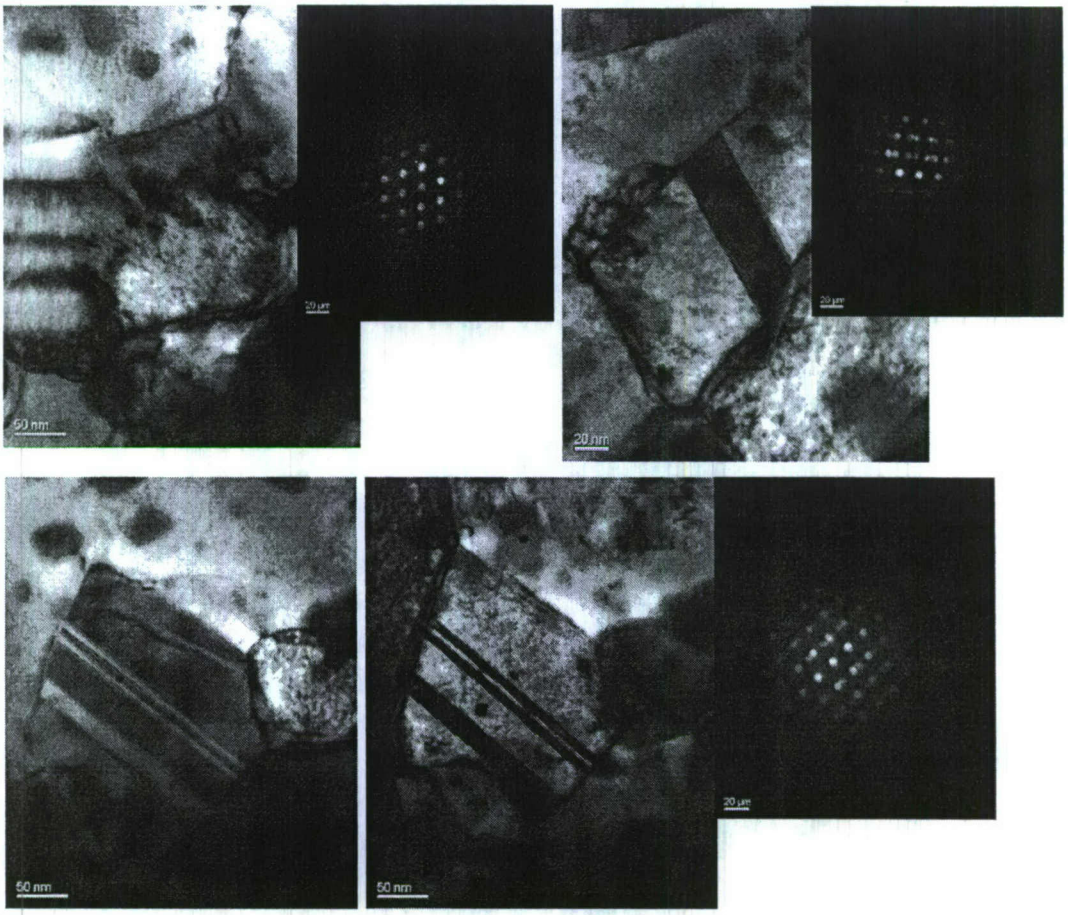

Figure 15: Equiaxed austenite grains in the shear band with a low dislocation density, coarse twins of the type {111}<11-2> and associated diffraction patterns to confirm their structure and twinning relationship.

In addition to equiaxed austenite grains, equiaxed grains of ferrite were also observed coexisting with the austenite. These grains appeared to be heavily twinned and one example is provided in Figure 16 along with diffraction patterns from different zone axes confirming the bcc structure. These grains are also approximately 200 nm in diameter. An analysis of the diffraction pattern corresponding to the [110] zone axis and the [012] zone axis confirmed that twinning is of the (11-2)<111> type (Figure 17). The bcc ferrite grains were also probed for composition using EDX spectra and they confirmed that they also formed in a diffusionless manner in that their composition was similar to that of the austenite grains and the overall alloy composition as well –i.e. ~12%Ni.

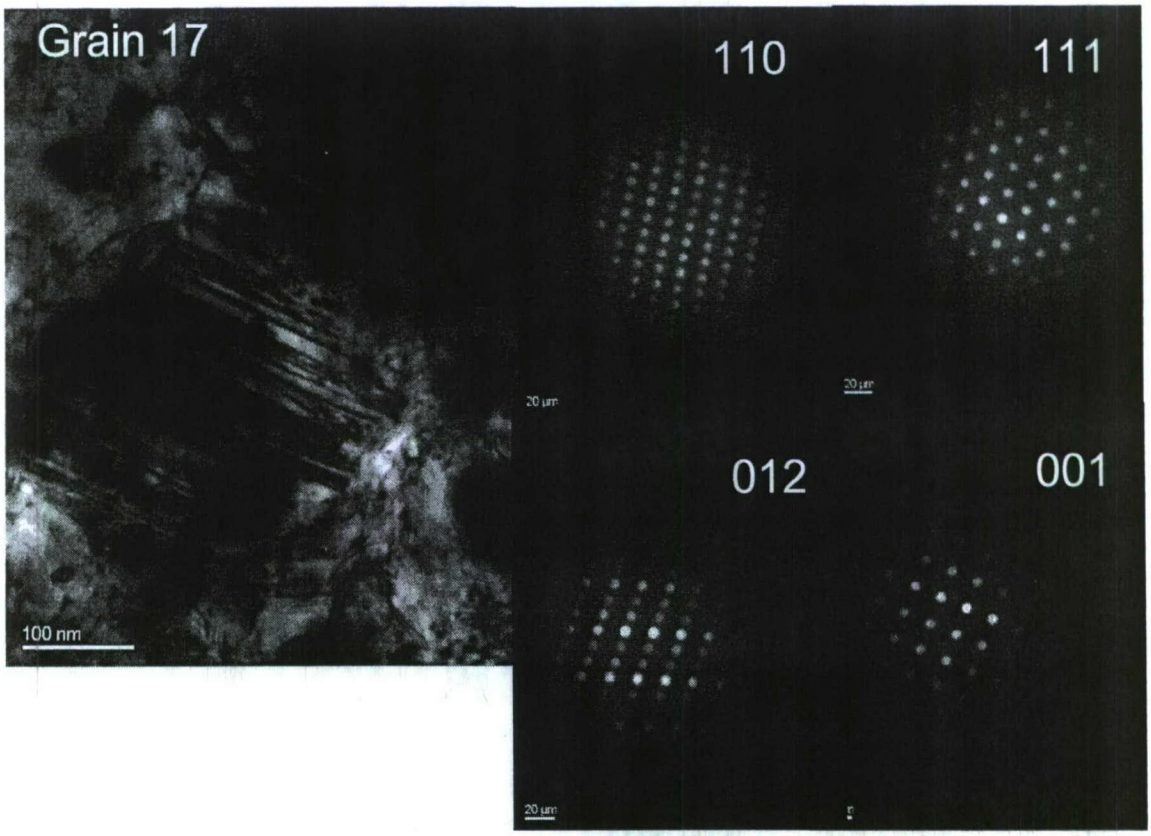

Figure 16: Heavily twinned equiaxed grains of ferrite with associated diffraction patterns confirming the bcc structure.

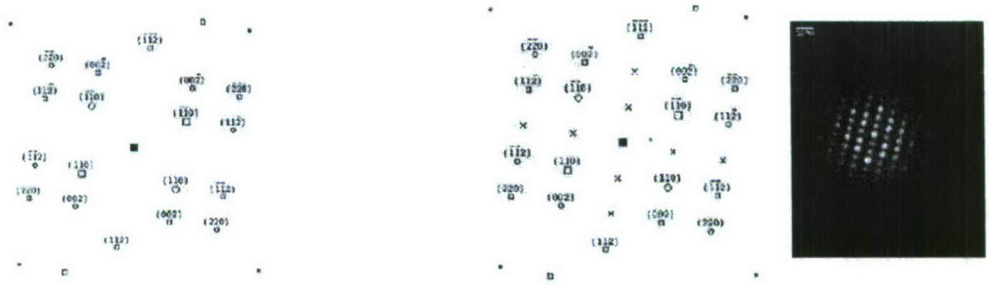

Figure 17a-c: (a) simulated [110] zone axis pattern incorporating (11-2)<111> type twinning without double diffraction effects. In (b), same as (a) but with double diffraction effects incorporated, and in (c) an experimental diffraction pattern using the [110] zone axis is shown.

The second approach involved mechanically grinding a fractured specimen down from the side away from the fracture surface and then precision ion polishing (PIP) the last 100 micrometer thick material using only a single gun (i.e. from one side) till a perforation appeared in the specimen. In this way, the fracture surface or regions very close to it could be examined in the TEM. This exercise is a lot more difficult than it appears since although the fracture morphology itself is microscopically flat, the surface has different heights at various locations with respect to a reference horizontal plane making it difficult to obtain a specimen of uniform thickness. Each sample takes two to three weeks to prepare and there is no guarantee that an electron transparent specimen will result. Nevertheless, repeated specimen preparation led to some success and the results are illustrated below. It is also pertinent to remember that the specimen obtained from the FIB (previous approach) was a small sliver (~ 5 x 5 micrometers) mounted on a copper grid and therefore, magnetic interactions and beam alignment within the TEM is minimal. In this second approach, the entire specimen is magnetic, making tilting experiments non-trivial.

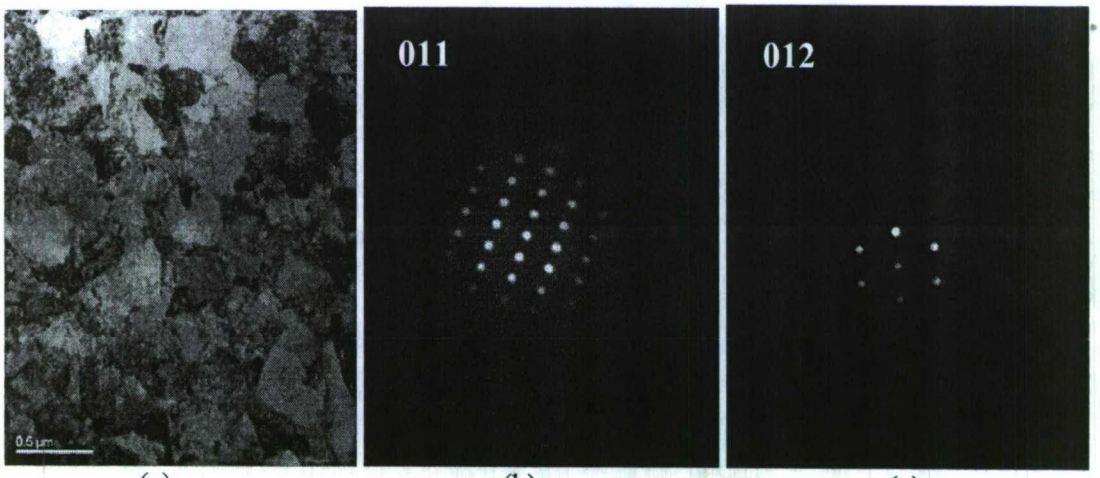

Figure 18a-c: Bright field image (a) showing highly dislocated equiaxed 200 nm grains adjacent to the fracture surface while the associated (b) [011] and (c) [012] zone axes diffraction patterns confirm the bcc structure.

A bright field image obtained from one such specimen (Figure 18a) confirms the presence of equiaxed grains approximately 200 nm in size; these grains look highly dislocated and when the specimen was tilted and microdiffraction was performed on various grains, they confirmed a bcc structure (Figures 18b,c). This would then

correspond to ferrite. Another striking feature was the absence of carbides within the grains. The latter would suggest that the carbides had dissolved in this region and that would allow carbon and carbide forming element like V, Ti, Mo and Nb to enter into solid solution. These elements may assist ferrite stabilization at high temperatures.

The microstructure within the equiaxed region was examined at very high magnifications using specimens that were extracted using a FIB (note that this would be very difficult to do with standard 3-mm TEM specimens due to the material being magnetic and interfering with the column alignment) and representative micrographs are provided in Figure 19. It should be mentioned that the images presented in Figure 19 are from a second FIB specimen where only ferrite grains were observed in the equiaxed region. Within the individual equiaxed grains, a fine scale modulated pattern is observed reminiscent of dislocation cells on the scale of approximately 20 nm, these being particularly evident in Figure 19c. In other grains, fine-scale twinning is noted, as is a high dislocation density (Figure 19d).

Fracture surfaces obtained from several of the specimens that exhibited cracking were examined in the SEM and representative micrographs from regions of the fracture are shown in Figure 20a,b. Whereas in some areas elongated dimples, characteristic of ductile shear failure are evident (Figure 20a), in other areas, a rather curious morphology is evident (Figure 20b); a substrate of equiaxed grains where the grain boundaries appear grooved is noted, and above this substrate are extensive streaks of metal that appear to traverse several grains, after originating either at grain interiors or grain boundaries and almost always terminating in a bulb. These are believed to be molten metal that streaked across the surface and solidified. These streaks appear to be of the order of 20-30 nm wide and a fraction of that in height, suggesting the presence of a very thin molten metal layer during shearing. Together, these microstructural features and the associated dynamic stress-strain curves present a coherent picture of this steel in this high strength condition being extremely prone to shear localization. Similar conclusions were reached by the Caltech group.

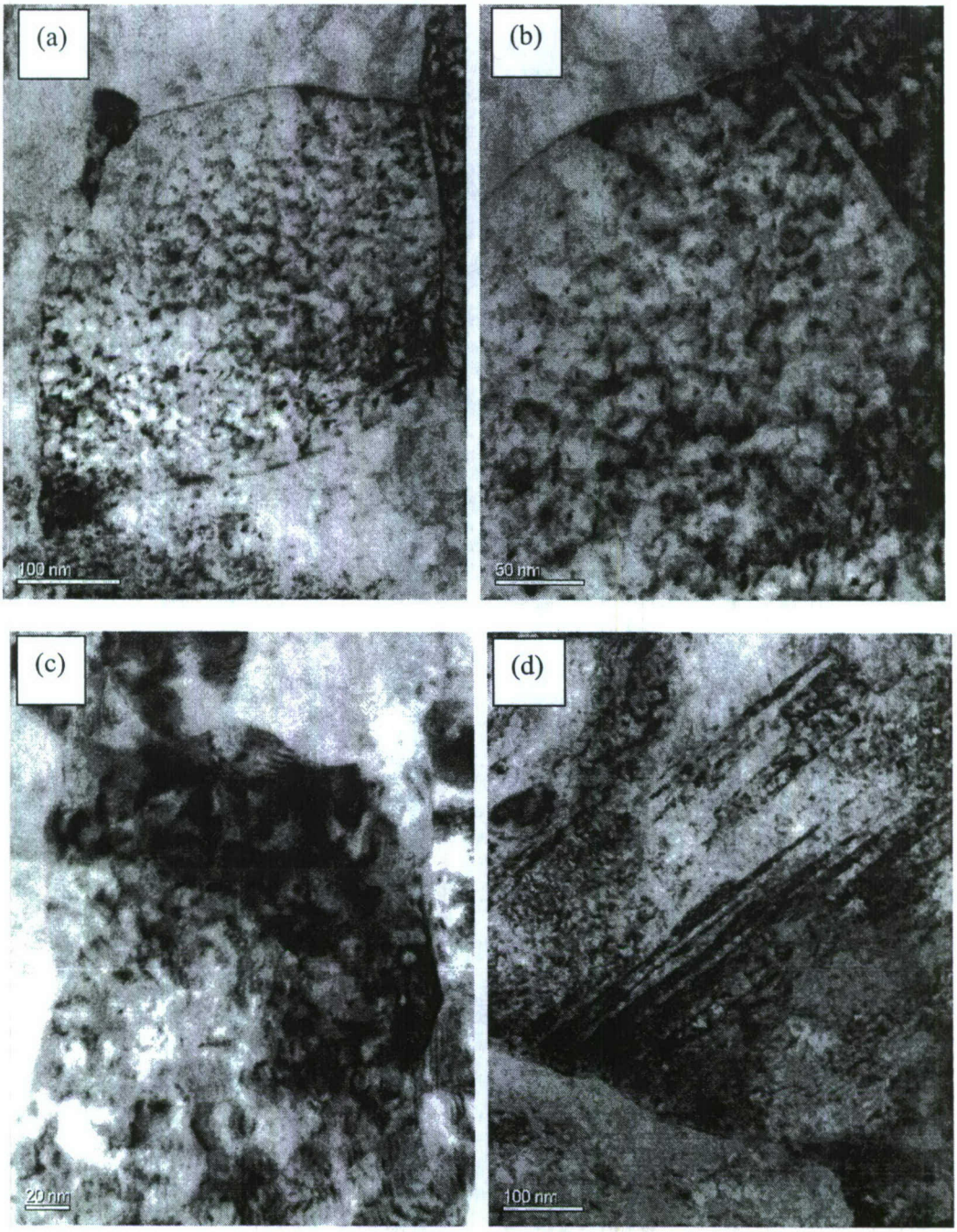

Figure 19: The fine structure within the equiaxed grains in the shear band showing what appears to be (a-c) 20 nm cells within the grains and d) fine scale twinning and high dislocation density.

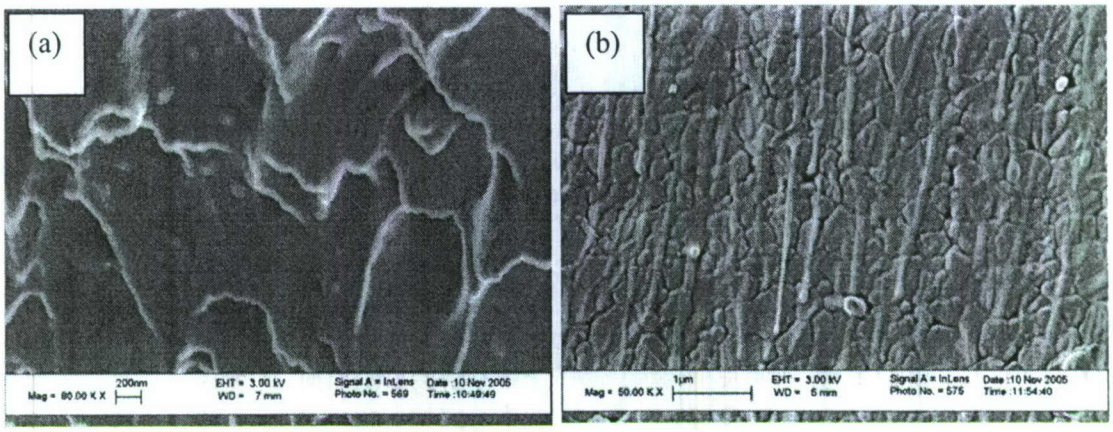

Figure 20a,b: Fracture surfaces from specimens that exhibited cracking during the dynamic compression tests. (a) shear dimpled rupture, and (b) indications of melting and streaking of the molten metal on the fracture surface. Note the fine equiaxed grain structure on the fracture surface just "below" the molten streaks and extensive grain boundary grooving resulting from wetting of the boundaries from the liquid metal.

Lastly, in order to probe the mechanical characteristics of the shear band, several nanoindentation traverses were made across the shear bands in a well-polished specimen with indentation spacing of the order of 2 micrometers (Figure 21). It is seen that between indentation numbers 19 and 28, the hardness increases from a background level of about 6.5 GPa to as high as 8.0-8.5 GPa. The high hardness region corresponds to the ASB as verified by post-indentation micrographs. Interestingly, this was not always the case and there were situations where the hardness of the ASB and the baseline hardness were similar.

It is also worth mentioning that we had established collaboration with the Dynamic Testing Group at Los Alamos National Laboratories (Drs. George T. (Rusty) Gray and Ellen Cerreta) who performed dynamic tests on the 10 Ni alloy using their "top-hat" specimen configuration and arrived at the same conclusion, i.e. the 10-Ni steel in the ultra-high strength condition is excessively prone to shear localization during dynamic deformation.

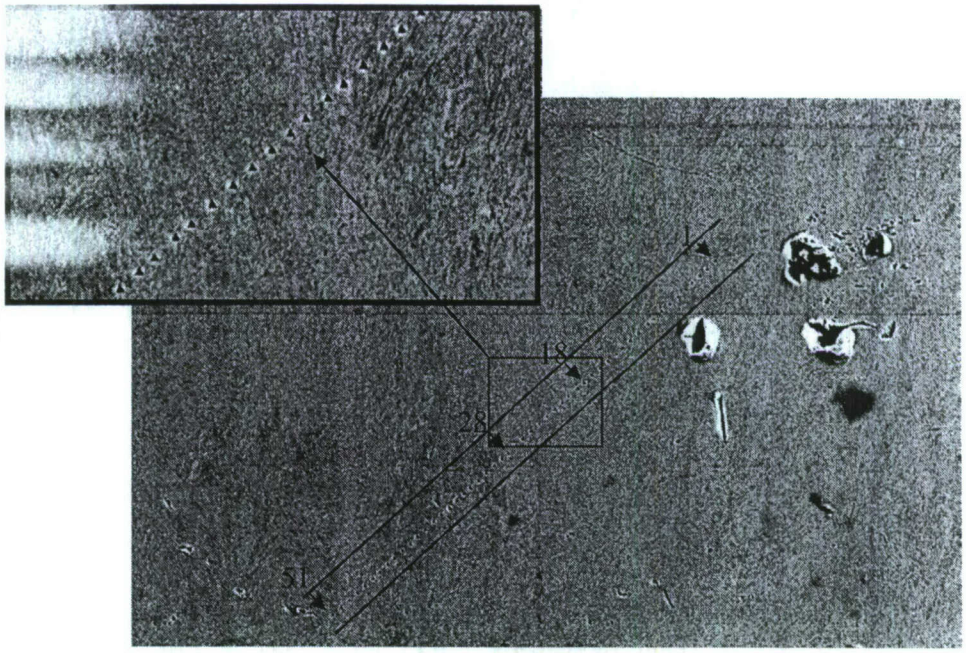

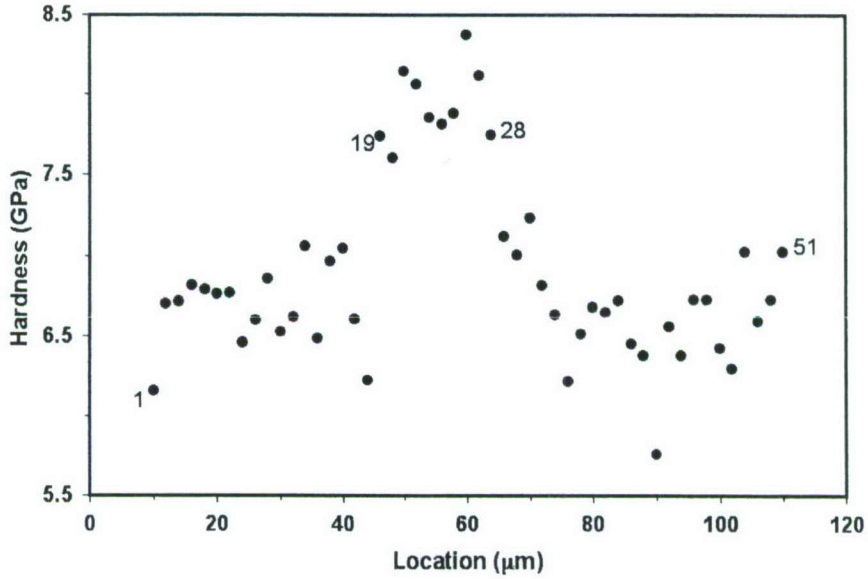

Figure 21: Nanoindentation profile across the shear band (note that indentations 19-28 traverse the shear band whereas the rest are in the relatively less-deformed regions in the specimen).

2.4 Deformation Response of HSLA-Comp 3 and HSLA-Comp 2

The acute propensity for the 10Ni steel to exhibit strain localization during dynamic deformation has caused technological interest in other high-strength steels with lower Ni content (2.0%Ni and 3.0% Ni rather than 10%Ni) and static yield strengths that are in the 120-130 Ksi range rather than 150-165 Ksi that is typical of the 10Ni steel in the optimally heat-treated condition. Here, we discuss the progress made in understanding the deformation behavior of one such steel, HSLA-Comp 3.

An optical micrograph of the HSLA-Comp-3 alloy in the as-received condition is presented in Figure 22. The microstructure appears martensitic but the scale is coarser than that observed in the 10 Ni steel. Examination of the microstructure in the TEM reveals the lath martensite microstructure, with the laths appearing somewhat coarser than those observed in the 10 Ni steel (Figure 23a,b). A high dislocation density is noted within the laths (Figure 23c) as is a fine fairly homogeneous distribution of second phase particles (Figures 23d,e). These include carbides as well as copper precipitates that are of the order of 10 nm or less in size. These particles are very effective in pinning dislocations (Figure 23f).

Figure 22: A representative optical micrograph of the as-received HSLA-Comp 3 steel showing a martensitic microstructure.

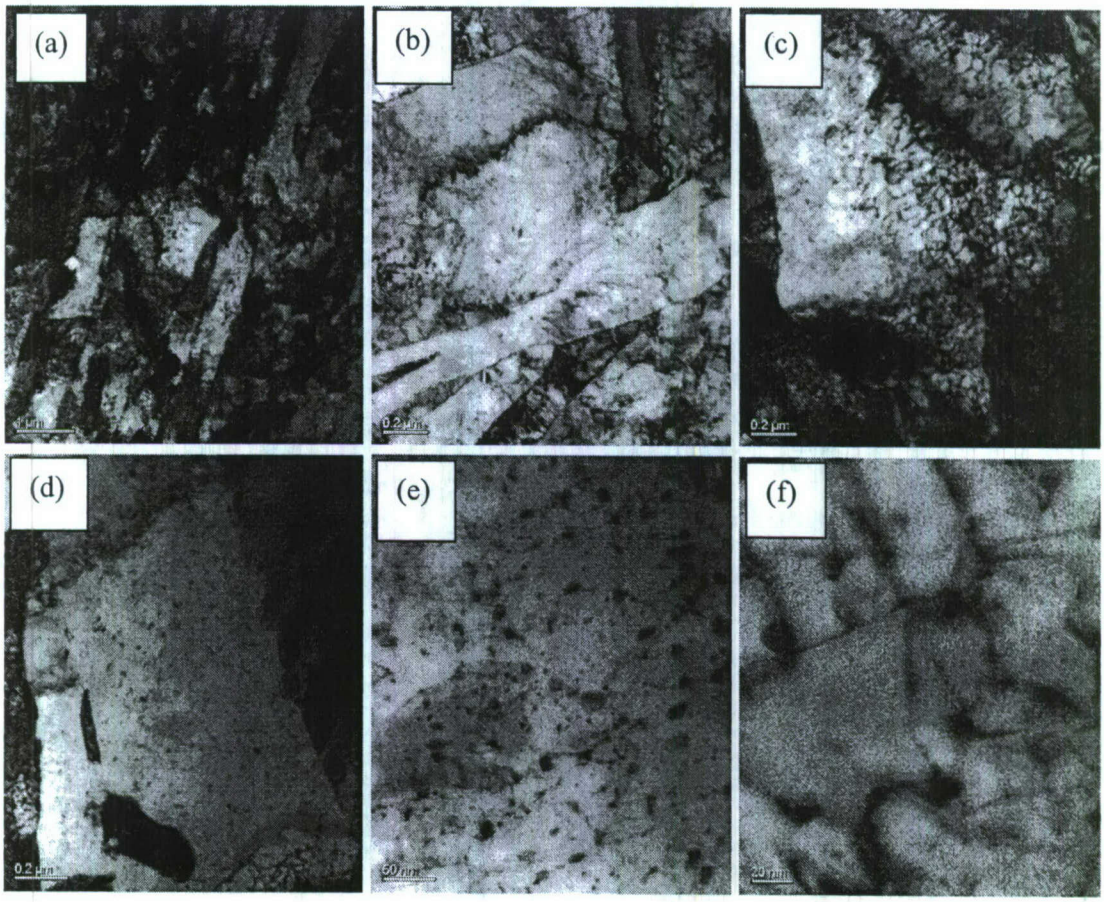

Figure 23: Microstructure (TEM) of HSLA-Comp 3 in the as-received condition: (a,b) Martensite laths, (c) High dislocation density within the laths, (d,e) fine carbides and Cu precipitates within the laths, and (f) dislocation pinning by the precipitates.

Quasi-static compression stress-strain curves at nominal strain rates of 1/s, 10^{-2}/s and 10^{-4}/s are shown in Figure 24a for the HSLA-Comp 3 specimens and it is clear that in this strain rate regime, the yield strength and early stage work hardening response are insensitive to strain rate. The stress-strain response for the HSLA-Comp 3 steel is compared against that for the 10 Ni steel at a nominal strain rate of 10^{-2}/s (note that in these figures, engineering stresses and strains are and so at larger strains, a geometric hardening due to increase in cross-sectional area is not accounted for) and it can be seen that the static yield strength for the 10Ni steel is around 1200 MPa whereas that for HSLA-Comp 3 was around 850 MPa; the quasi-static work hardening rates are however similar.

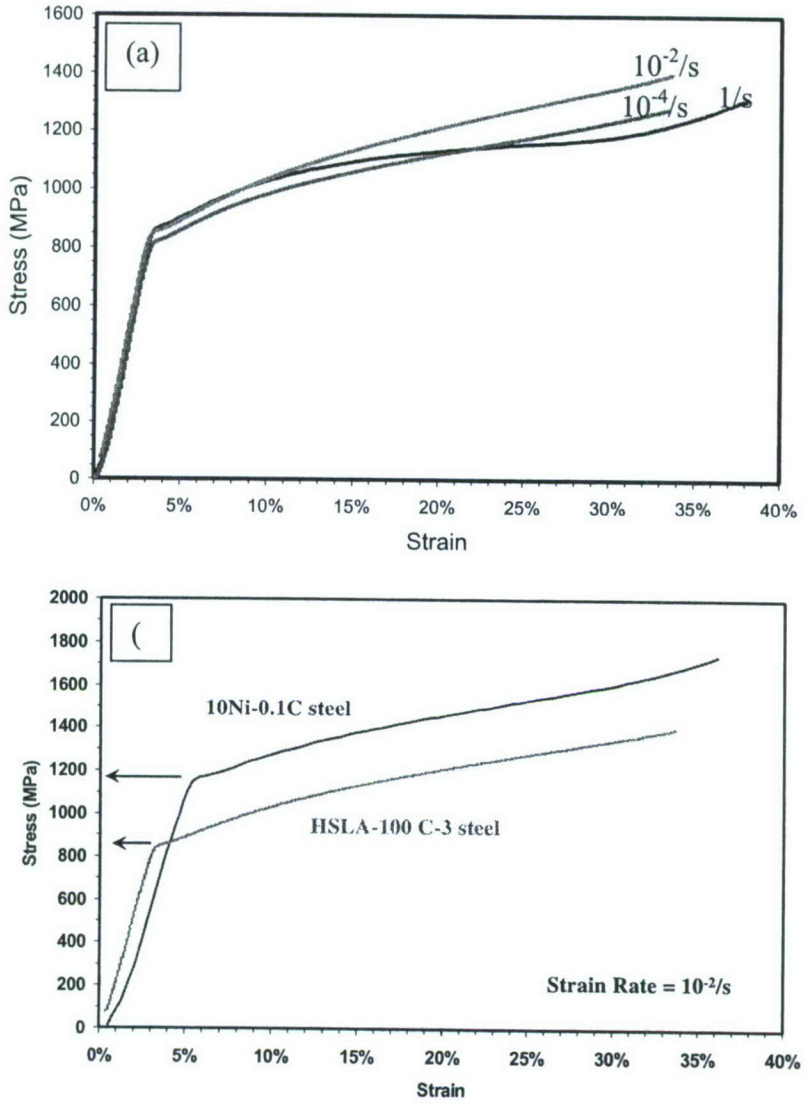

Figure 24: Compressive engineering stress-strain curves for HSLA-Comp 3 at quasi-static strain rates, and (b) a comparison of the stress-strain curves for HSLA-Comp3 versus the 10 Ni steel at a nominal strain rate of 10^{-2}/s.

The deformed microstructure following the compression tests at a nominal strain rate of 10^{-2}/s for the HSLA-Comp 3 specimen is shown in Figure 25a,b and it can be seen that in the orientation of maximum shear the grains are extensively elongated, more so for the specimen with a height strain of 50% (Figure 25b) versus that for a specimen with a height strain of 30% (Figure 25a). The microstructure of the specimen deformed to 50% height strain was further examined in the TEM and representative micrographs are shown

in Figures 25c-e. The martensite laths are well-defined, and appear reoriented much like in the 10Ni steel, refined in lath width and heavily dislocated (Figures 25c,d).

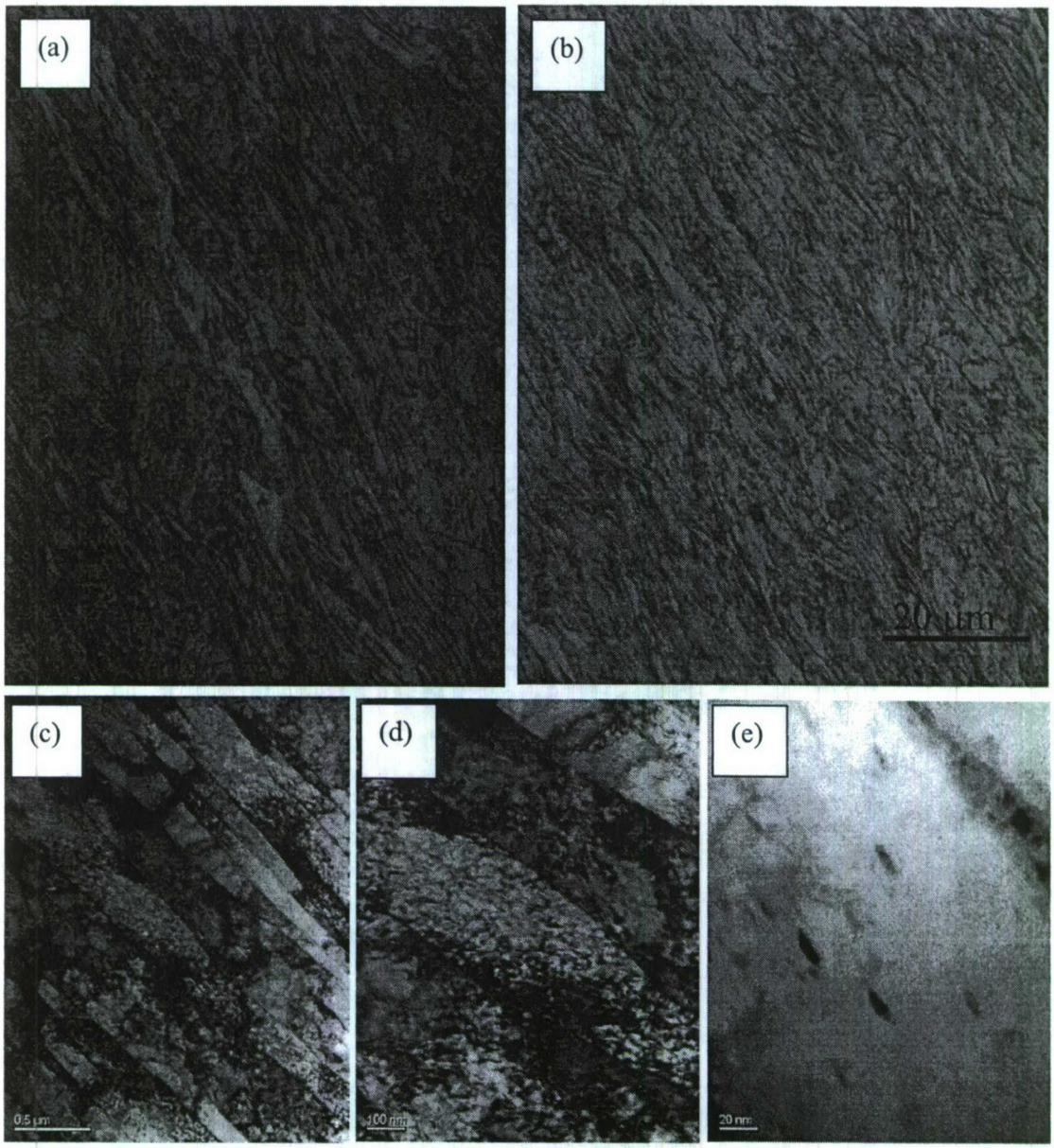

Figure 25: Deformed microstructure in the HSLA-Comp 3 specimens following quasi-static compression at a strain rate of 10-2/s to a height strain of (a) 30%, and (b-e) 50%. (b) is an optical micrograph whereas (c-e) are TEM bright field images showing the deformed microstructure.

A careful examination of the microstructure within the individual laths confirms that the Cu precipitates are no longer equiaxed but elongated along the shear orientation

confirming they plastically deform along with the matrix. These observations were also true in the specimen that was deformed at the same strain rate to the lesser extent of 30% height strain (Figure 25a).

Dynamic Deformation of the HSLA-Comp 3 steel was carried out using the compression Kolsky bar (Split Hopkinson) in a manner analogous to the 10Ni steel. Interestingly, for all the strain rates and height strains examined, shear localization did not occur in this steel. As an example the engineering stress-strain curve for a HSLA-Comp3 specimen tested at a strain rate of 3500/s is compared to that of a 10Ni steel response at a strain rate of 2500/s. It is clear from Figure 26a that the 10Ni steel is stronger than the HSLA-Comp 3 in dynamic compression, work hardens similarly but is prone to localization, whereas the Comp3 still continues to deform homogeneously to large strains. In order to encourage localization in the HSLA-Comp 3 steel (so that microstructural evolution in the shear band could be examined and understood), a notch was cut into the two opposite corners of the cuboidal compression specimens (along the diagonal shear plane) and then deformed using the Kolsky bar setup. The resulting engineering stress-engineering strain curve is compared to a similar test but without the notch machined in, in Figure 26b. Note that the curve for the notched specimen is only shown up to the location where shear localization was initiated but nevertheless it did not propagate much and beyond that, the specimen continued to deform homogeneously to over 70% height strain! This should be contrasted against the 10Ni specimen where, once such a shear band nucleated, it propagated rapidly across the entire specimen at even slower strain rates and the specimen cracked into pieces.

The resulting microstructure from the notched specimen is shown in Figure 27a where the diffuse shear band is readily observed. TEM specimens were extracted from the shear band and examined and representative micrographs are shown in Figures 27b-e. Unlike in the 10 Ni steel, within this band, equiaxed grains are not observed; instead the laths appear elongated and the precipitates inside the laths and at lath boundaries (carbides and Cu) appear intact. Thus the severity of localization from a microstructural point of view is considerably less in this steel.

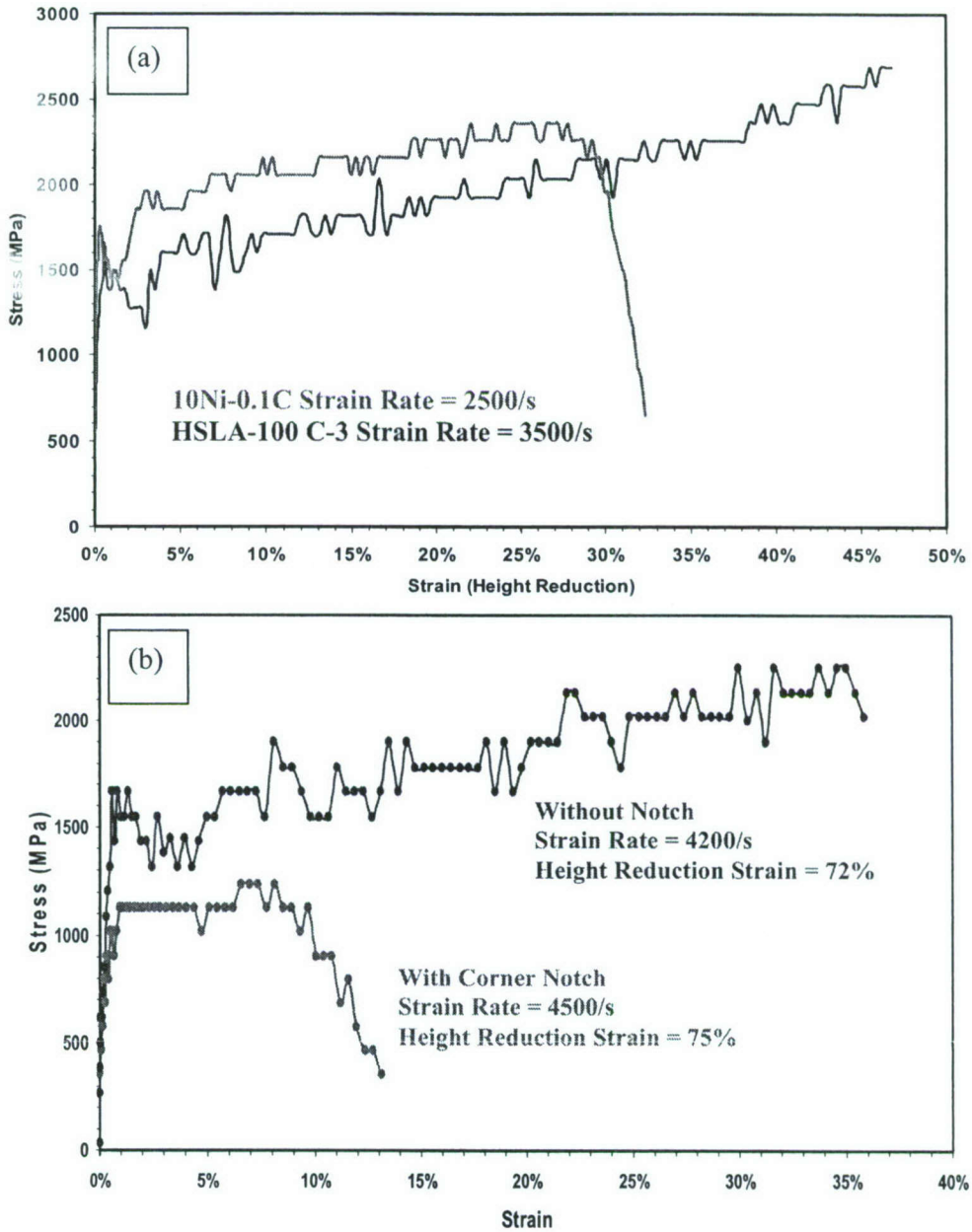

Figure 26: (a) Dynamic compression response of the HSLA-Comp 3 steel versus the 10 Ni steel, and (b) stress-strain curves for HSLA-Comp 3 specimens with and without a notch machined into the specimens.

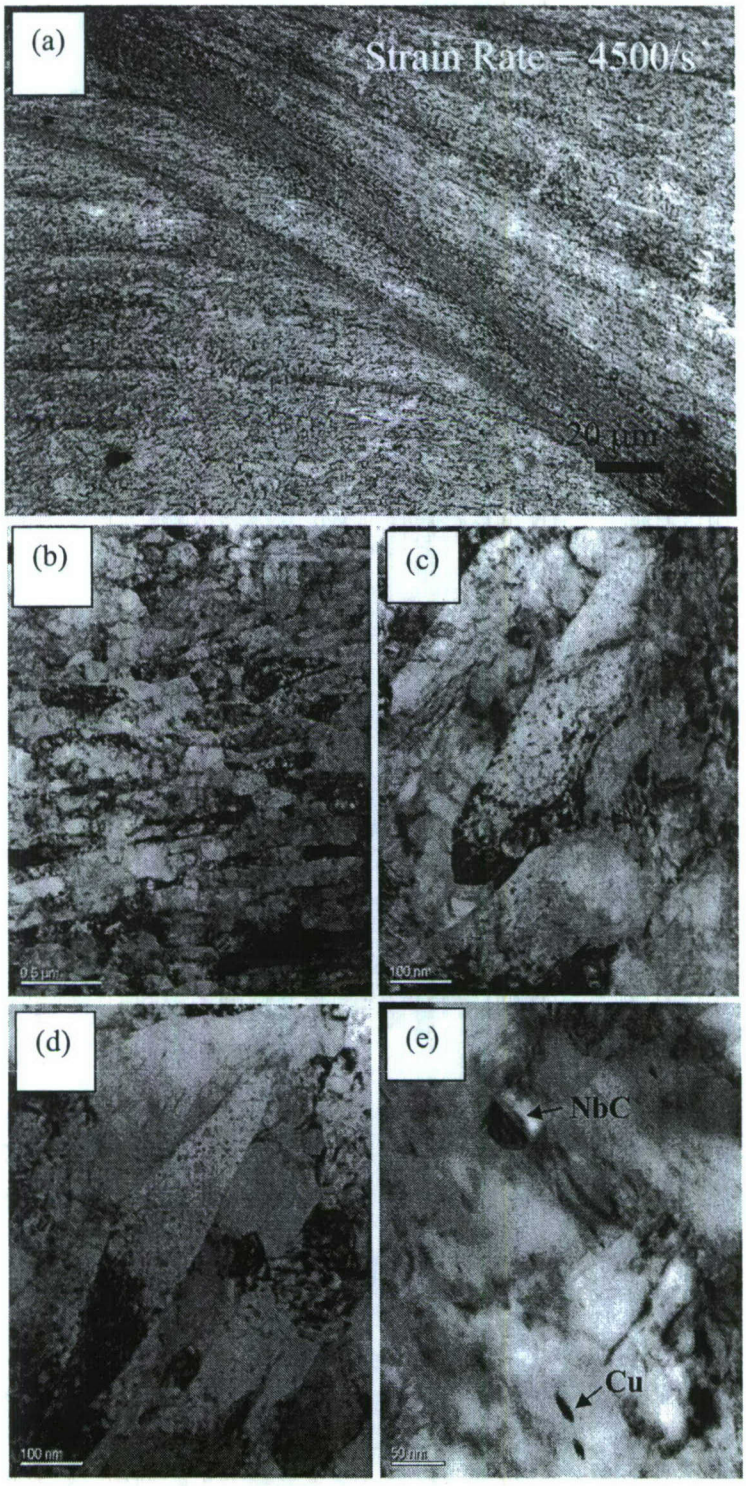

Figure 27: (a) Optical micrograph of the diffuse shear band in the notched HSLA-Comp 3 specimen and (b-e) corresponding TEM micrographs showing the lath structure, the high dislocation density and the preservation of the precipitates within the laths.

3.0 Conclusions

A. The 10Ni steel in the fully heat-treated condition is more susceptible to localization and ASB formation compared to HSLA C2 and C3.

(i) In the 10 Ni steel, within the ASB, a central equiaxed structure is observed, the equiaxed grains being 0.2-0.4 mm in size.

(ii) The equiaxed grains are composed of primarily ferrite with a high dislocation density (and sometimes twinning) but occasionally austenite grains with a low dislocation density were observed in FIBed specimens.

(iii) High magnification imaging suggests the presence of a cell structure within the equiaxed ferrite grains that are ~20 nm in size.

(iv) Fracture surfaces from failed specimens confirmed regions of melting in addition to shear dimpled rupture.

(v) Carbides were rarely observed within the shear band in the equiaxed region, and when they were, they appeared smaller than those away from the shear band.

(vi) The martensite lath size in the ASB flanking the central equiaxed region appeared to have more or less the same size distribution as those observed in the quasi-statically deformed specimens and significantly refined compared to the undeformed specimen.

B. Using the compression Kolsky bar set-up, we were unable to generate ASBs in the HSLA-Comp3 alloy.

(i) At strain rates as high as 4500/s, the compression specimens deformed homogeneously to height strains of 75%.

(ii) Notching the specimen enabled localization but the process decayed and further deformation occurred homogeneously.

(iii) Within the localized region, equiaxed grains were not observed; carbides and Cu particles were present and the particles were effective in pinning dislocations.

(iv) The Cu particles deform plastically and appear elongated but no more so than those observed after quasi-static deformation.

C. The microstructure within the localized deformation band in the HSLA-Comp2 material obtained from NSWCCD (V50 specimen) appeared fairly similar to what we observed in the HSLA-Comp3 specimens.

4.0 References

1. K. Cho, Y.C. Chi and J. Duffy, Metall. Trans., 21A, 1161 (1990).
2. H.C. Rogers, Ann. Rev. mater. Sci., 9, 283 (1979).
3. M.E. Backman and S.A. Finnegan, in Metallurgical Effects at High Strain Rates, editors: R.W. Rohde et al., Plenum Press, New York, NY, 1973 p. 531.
4. K-M. Cho, S. Lee, S.R. Nutt and J. Duffy, Acta Metall. Mater., 41, 923 (1993).
5. P.R. Guduru, G. Ravichandran and A.J. Rosakis, Physical Review E, 64, 036128 (2001).
6. D.E. Grady, JMPS, 40, 1197 (1992).
7. G. Gioia and M. Ortiz, JMPS, 44, 251 (1996).
8. C.M.Glass, G.M.Moss and S.K.Golaski: Response of Metals to High Velocity Deformation, eds. P.Shewman and V.F.Zackey, New York, 1961, 115.
9. L.E. Murr, E.V. Esquivel, Observations of common microstructural issues associated with dynamic deformation phenomena: Twins, microbands, grain size effects, shear bands, and dynamic recrystallization. J. Mater.Sci., 39(2004)1153
10. L.E. Murr and C. Pizana, Dynamic Recrystallization: The Dynamic Deformation Regime. Metall. Mater. Trans. A 38 (2007)2611
11. M.C.Mataya, M.J. Carr and G. Krauss, Flow localization and shear band formation in a precipitation strengthened austenitic stainless steel. Metall. Mater. Trans. A13(1982)1263
12. L.E. Murr, C.S. Niou and C. Feng, Residual microstructures in explosively formed tantalum penetrators. Scripta Mater. 34(1994)297
13. M.A. Meyers, Y.B. Xu, Q. Xue, M.T. Perez-Prado and T.R. McNelley, Microstructural evolution in adiabatic shear localization in stainless steel. Acta Mater. 51(2003)1307
14. L.E. Murr and K.P. Staudhammer and S.S. Hecker. Effects of Strain State and Strain Rate on Deformation-Induced Transformation in 304 Stainless Steel: Part II. Microstructural Study. Metall. Mater. Trans. A (1982)627
15. J.A. Hines, K.S. Vecchio and S. Ahzi. A model for microstructure evolution in adiabatic shear bands. Metall. Mater. Trans. A 29 (1998)191
16. F. Martinez, L.E. Murr, A. Ramirez, M.I. Lopez and S.M. Gaytan Dynamic deformation and adiabatic shear microstructures associated with ballistic plug formation and fracture in Ti–6Al–4V targets. Mater.Sci.Eng. A.454-455(2007) 581
17. J.F.C. Lins, H.R.Z. Sandim, H.-J. Kestenbach, D. Raabe and K.S. Vecchio, A

microstructural investigation of adiabatic shear bands in an interstitial free steel. Mater.Sci.Eng. A.457 (2007) 205
18. Q.Xue, J.F. Bingert, B.L. Henrie and G.T. GrayIII, EBSD characterization of dynamic shear band regions in pre-shocked and as-received 304 stainless steels. Mater.Sci.Eng. A473 (2007) 279
19. M.T. Perez-Prado, J.A. Hines and K.S. Vecchio, Microstructural evolution in adiabatic shear bands in Ta and Ta–W alloys. Acta Materialia, 49(2001)2905
20. K.Kad, J.M. Gebert, M.T. Perez-Prado, M.E. Kassner and M.A Meyers, Ultrafine-grain-sized zirconium by dynamic deformation. Acta materialia,54 (2006) 4111.
21. F. Duflos and B. Cantor, Microstructure and kinetics of martensite transformations in splat-quenched Fe and Fe-Ni alloys - I pure Fe: Acta Metallurgica 30(1982)323.
22. Y. Inokuti and B. Cantor, Microstructure and kinetics of martensite transformations in splat-quenched Fe and Fe-Ni alloys - II Fe-Ni alloys: Acta Metallurgica 30(1982)343.
23. Y. Inokuti and B. Cantor, The formation of martensite in splat-quenched Fe-Mn and Fe-Ni-C alloys: Journal of Materials Science 12(1977)946.
24. C. Hayzelden, J. J. Rayment and B. Cantor, Rapid solidification microstructures in austenitic Fe-Ni alloys: Acta Metallurgica 31(1982)379.